SPS LARGE ARRAY SIMULATION

S. Rathjen B. R. Sperber, E. J. Nalos, Boeing Aerospace Company

1.0 INTRODUCTION

The computer simulation has been developed with the objective of producing a flexible design and verification tool for the SPS reference design. The computer programming efforts have been directed primarily to beam pattern analysis. The following reasons have been specified as the purpose of the computer programs: verification of the reference design, definition of feasible departures such as quantized distributions, the study of far-out sidelobe roll-off characteristics, the analysis of errors and failures, illumination function analysis to develop beam patterns for efficient collection, and beam shaping synthesis to meet environmental constraints.

2.0 ARRAY SIMULATION PROGRAMS

Three types of computer simulations have been developed to study the SPS microwave power transmission system (MPTS). The radially symmetric array simulation is low cost and is utilized to investigate general overall characteristics of the spacetenna at the array level only. "Tiltmain," a subarray level simulation program, is used to study the effects of system errors which modify the far-field pattern. The most recently designed program, "Modmain," takes the detail of simulation down to the RF module level and so to date is the closest numerical model of the reference design.

Early in the computer program development stage, radially symmetric array simulations were written to model various power taper distributions and to compare their beam efficiencies.

The radially symmetric simulations have been used to study a variety of spacetenna distribution functions enabling comparisons of the on-axis power densities, the far field patterns, and their associated beam efficiencies.

The "Tiltmain" array simulation is much more complex than the circularly symmetric simulation due to the fact that "Tiltmain" models the spacetenna as comprised of 7220 subarrays. In "Tiltmain," the ground-grid is specified as a planar circular area where the electric fields are determined. The field at any particular point on the grid is computed using scalar wave equations with approximations that make them accurate in the Fresnel Zone. The equations are not valid for the very near field, but give very good results in the Fresnel Zone, $D^2/\lambda > R > 2D^2/\lambda$, and the far field $R > 2D^2/\lambda$ where D is the diameter of a circular spacetenna or the diagonal of a rectangular spacetenna, λ is the wavelength of the transmission signal, and R is the range from the spacetenna to the ground-grid. The electric field at any particular point is determined by calculating the field from each subarray in the spacetenna to the given grid point and then summing all the fields to give the total field at that grid point.

The total power collected by the ground-grid is calculated by multiplying the power density at a point by the incremental area associated with that point to give the power over that area, and then summing up the power from each sample. Efficiencies with respect to the total power collected on the ground-grid and with respect to the total input power of the orbiting spacetenna are calculated at incremental grid distances out of the specified diameter.

"Modmain" is the most complex simulation of the MPTS to date in that the spacetenna is modelled not only as 7220 subarrays (as in "Tiltmain") but each subarray is modeled as a composition of RF transmitter modules. "Modmain" models over 100,000

modules and simulates phase errors, amplitude errors, failures, and systematic as well as random tilt.

The "Tiltmain" simulation was unable to model below the subarray level because its program structure caused data storage limitations problems; "Modmain" is structured in such a way as to overcome this disadvantage. Previously, the amplitude and phase of each subarray was stored in an array and recalled for each ground point. With "Modmain" the amplitude and phase of every module is not stored but the contribution of a module at each ground point is calculated and stored before moving on to the next module where the contribution is added to the previous ground point contributions.

3.0 REFERENCE DESIGN VERIFICATION

The computer programs have been used to investigate different antenna aperture illumination functions. An optimized aperture distribution will maximize the RF power intercepted by the ground rectenna and minimize the sidelobes and grating lobes. The types of illumination functions investigated include: Gaussian, cosine on a pedestal, uniform, reverse phase, inflected Bessel, and quadratic on a pedestal. Each of these was evaluated in terms of maximum power density at the transmit array and the rectenna, sidelobe levels, beam shape, and beam efficiency. Several Taylor series tapers were also explored with general results indicating that sidelobe levels decrease as the amount of taper increases.

Figure 1 shows five spacetenna distribution functions and the required spacetenna size and power densities to produce the same peak power density on the ground and the same size main beam. Figure 2 depicts the five far-field patterns showing the relative levels of the sidelobes. It was found that a 10 dB Gaussian taper has the best performance and that when quantized into at least eight levels produced nearly the same results as a theoretical continuously variable function. From antenna layout considerations, a 10-step, 10 dB Gaussian taper was then chosen for the aperture illumination (See Figure 3). The farther out sidelobes were compared for the continuous and ten-step quantized Gaussian tapers. The results show very little difference between the two cases.

In order to verify the energy distribution at distances far away from antenna boresight, it was necessary to determine the roll-off characteristics of the entire antenna. This was done by a numerical integration technique applied to the radiation pattern of the 10 dB Gaussian taper distribution. It was established that the sidelobes rolled off at 30 dB/decade of angle. This coincidentally is the roll-off rate of a uniform circular aperture. Next, the error plateaus were computed from the assumed error magnitudes and the number of subarrays associated with three different subarray sizes. The aperture efficiency was also obtained by numerical integration. Next the subarray roll-off characteristics were obtained by numerically integrating the square aperture distribution for each of 19 different cuts over a 45° sector of $\emptyset$. These cuts were then averaged at each θ. The resultant subarray sidelobes also roll off at 30 dB/decade of angle. There is an additional error plateau associated with the randomly scattered power by each slot in the subarray. This second plateau will in theory roll off in accordance with the radiation pattern of the slot.

The lowest integral element in the MPTS is the klystron module, composed of a klystron, its feed and radiating waveguides, thermal control, solid state driver and RF control, power distribution, power return, and the support structure. The factors in selecting the klystron module sizes include: RF power density and thus the thermal environment, ease of quantizing the spacetenna aperture distribution, and awareness of klystron module interfaces. The high power density at the center of the beam is generated by 36 klystrons, each rated 70 KW, radiating RF from an area slightly larger than 108 m^2 (area of subarray). The 36 klystrons are organized into a 6 by 6 matrix. At the edge of the 10 dB tapered antenna a

subarray should have 3.60 klystrons. Since 3.60 is not an integer number, each edge subarray has 4.0 klystrons formed into a 2 by 2 matrix. Matrix configurations were similarly established for each power density step in the taper. Due to the klystron module system interfaces and the thermal limitations, the smallest possible size module is 1.5 by 1.5 meters.

The reference system calls for phase control at the klystron module level. Current thinking defines this level rather than phase control at the subarray level because of the belief that the modules cannot be assembled together accurately enough to retain a uniform phase front. The uniform phase front for the subarray could not be achieved due to the tilt of the modules and the distributed phase errors which occur within the subarray. Figure 4 shows the comparison between subarray and klystron module phase control level as a function of random tilt. The peak power density on the Earth is closely correlated to the beam efficiency and so Figure 4 shows that the klystron module phase control level is significantly better than subarray level control.

Simulations made to compare phase control level as a function of random phase error is shown in Figure 5. The results indicate a range of values for both systems, meaning that for 10^{o} of random phase error both phase control systems have a random range of values statistically which are equal as would be expected.

Grating lobes are peaks in radiation occuring at angular directions off axis of the spacetenna where the signals from each of the subarrays add in-phase. The lobe amplitudes are a function of the mechanical alignment of the modules and the spacetenna pointing whereas the spatial position of the lobes is dependent upon the modules sizes. When there is no mechanical misalignment (no tilt of modules or spacetenna), the grating lobes appear to be split because the peaks of the "array factor" fall directly in the nulls of the subarray pattern. As tilt occurs, the peaks move out of the nulls, quickly increasing their amplitude because of the steep slope of the subarray pattern nulls. Figure 6 shows a comparison between grating lobe amplitudes for module and subarray phase control levels when two arc minutes of spacetenna tilt is simulated. Once again phase control at the module level shows a significant advantage over control at the subarray level.

4.0 SHAPED BEAM SYNTHESIS

In order to improve the overall collection efficiency by increased beam flatness out to the rectenna edge as well as provide an additional means of sidelobe control, beam synthesis with resultant phase reversals at some portions of the spacetenna was considered. These phase reversals are obtained by a fixed phase shifter at the klystron input and represent a first step towards a continuously variable phase distribution across the spacetenna, should this be more desirable. The results indicate that it is possible to synthesize a pattern that is considerably more flat-topped than the 10 dB Gaussian or other patterns that we have investigated. The price paid for this improvement is increased spacetenna size or a larger rectenna.

It is possible to increase the flatness of the beam without limit with arbitrarily large apertures and large numbers of beam components. Figure 7 compares the 10 dB Gaussian taper with the reverse phase taper and the continuous phase synthesis. The comparison shows the differences in the amplitude and phase illumination tapers across the spacetenna as well as the far-field patterns. Results show that reshaped beam pattern with "squarred" main beams are possible but at the expense of larger transmit antennas or larger rectennas.

The idea of adding a suppressor ring to the spacetenna was investigated in the hope of significantly reducing the first sidelobe level. Figure 8 presents the results of this

study. The upper left diagram shows the layout of the spacetenna with its uniform distribution out to 0.72 times the normalized radius and the suppressor ring of width W. The diagram on the upper right shows the linear relationship between beam efficiency and the first sidelobe level as the ring width changes. .98 R_o means that the width of the suppressor ring is bound by the edges .98 R_o and R_o. Looking at the lower right diagram shows the effect of changing the phase of the suppressor ring as well as the ring width. From this diagram it may be concluded that an in-phase ring is better than one which is out of phase. The lower left diagram shows the far-field pattern produced for the suppressor ring case where the inside edge of the suppressor ring is at .94 R_o. Although the first sidelobe is lower by about 5 dB than the case without a suppressor ring a significant loss in beam efficiency accompanies this achievement.

A dual suppressor ring case was looked into with a 10 dB taper rather than the uniform illumination and a larger spacetenna radius of 2 km. Figure 9 presents the illumination across the large array with the ring closest in out-of-phase by 180^o and the second ring in-phase with the array. The far-field pattern for this case is shown in Figure 10 with a sidelobe level about the same as the referenced design but a main beam radius which is about 2.35 Km less.

A study was made to look at using defocusing and phase taper for beam shaping. Cases where the beam was focused at infinity showed much lower peak power density and much broader beams. These results indicate that reshaped beams with reduced peak levels are possible at the expense of larger spacetennas or rectennas.

Quadratic phase taper was utilized to look at shaped beam synthesis. In Figure 11, the far-field patterns for 4 cases with uniform amplitudes and different quadratic phase tapers are compared. As $\emptyset$ max increases the on-axis power density decreases (see Figure 11) and the beam efficiency decreases significantly (see Figure 12). Figures 13 and 14 show the far-field patterns and efficiencies for quadratic phase taper with the Gaussian rather than the uniform amplitude taper. These results show that the reference Gaussian taper without quadratic phase error is the most efficient pattern. Figure 15 presents a table which shows how the quadratic phase taper may be utilized to design alternate SPS systems.

5.0 SPS SYSTEM SIMULATION

In this final section three types of SPS system simulations are described: a) Incoherent phasing, b) startup/shutdown operations, and c) multiple beams. Incoherent phasing was simulated to investigage the effect of complete phase control failure. The results show that the far-field pattern takes on a constant value in the rectenna and sidelobe region. The constant value is about .003 mw/cm^2 over 5 dB below the Russian exposure level.

Computer simulations were utilized by JSC to investigate the performance of the MPTS during startup/shutdown operations. (See paper by G. D. Arndt and L. A. Berlin entitled "Microwave System Performance For A Solar Power Satellite During Startup/Shutdown Operations" on p. 1500 in Vol. II of the Proceedings of the 14th Intersociety Energy Conversion Engineering Conference.) Three sequences are recommended--random, incoherent phasing, and concentric rings-center to edge. The use of incoherent phasing is attractive in that it allows the antenna to be energized in any sequence. In conclusion the question of energizing the antenna has several practical solutions and should not present environmental problems.

The possibility of transmitting several power beams from an SPS has intrigued various researchers for some time. Recently, some computer runs were made to verify the capability of transmitting multiple beams using a modified version of the large array program TILTMAIN. The scheme used to generate the beams was the simplest possible

one imagineable; namely, splitting the main beam along an axis by spatially modulating the illumination function by a factor cos (k r sin θ) when: $k = 2\pi/\lambda$, r = subarray displacement from center, θ = beam split angle. Results of a simply split 6.5 G.W. reference Gaussian are shown on Figure 16, and are as predicted except for the central lobe which did not diminish as the split angle was increased to 6×10^{-4} radians. The central peak may be due to an in-phase residual component in the spatial modulation or a grating lobe effect. Understanding and eliminating the central peak will be among our future efforts along with investigating various other multiple beam effects.

6.0 CONCLUSION

The computer simulations described have proven to be powerful versatile tools in the prediction of RF performance of the space solar power satellite. They are continually being refined and their use is being extended into the planning of initial experimental verification of the array performance.

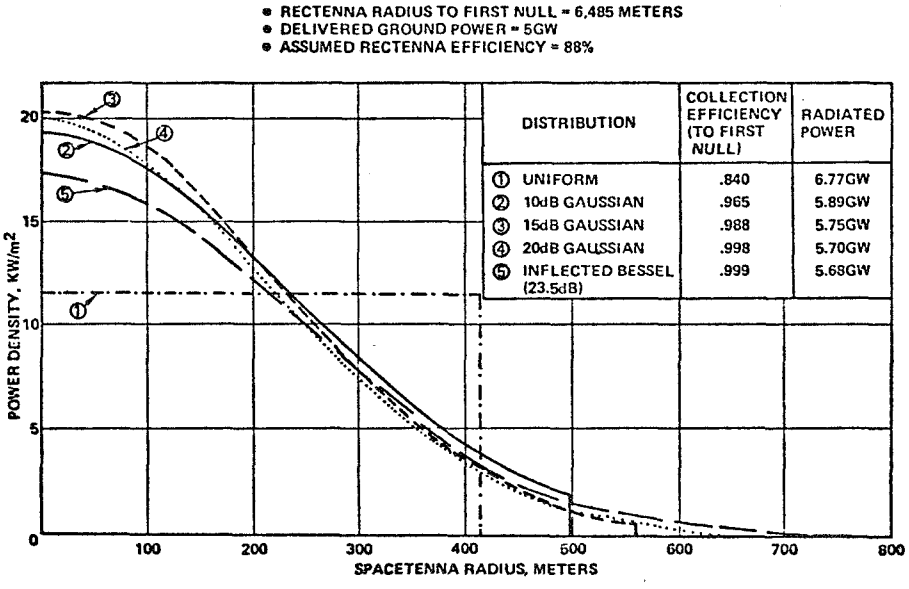

FIGURE 1

FIGURE 2

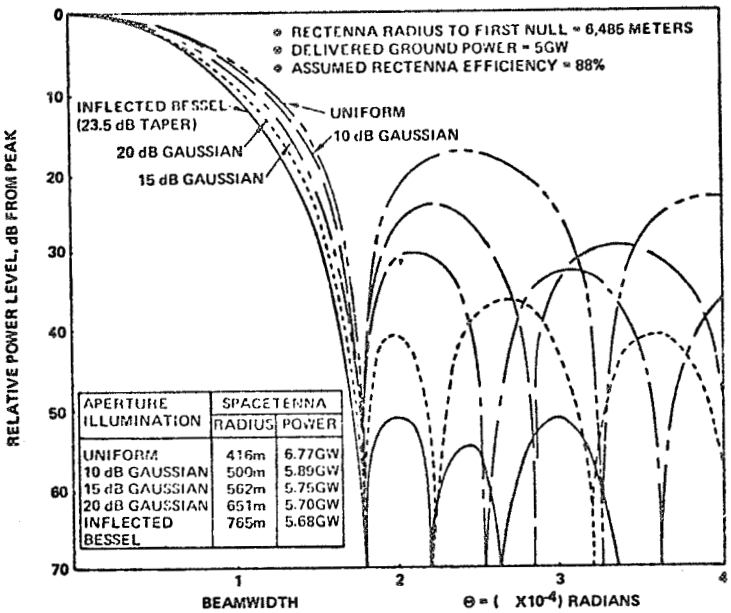

APERTURE ILLUMINATION	SPACETENNA RADIUS	POWER
UNIFORM	416m	6.77GW
10 dB GAUSSIAN	509m	5.89GW
15 dB GAUSSIAN	562m	5.75GW
20 dB GAUSSIAN	651m	5.70GW
INFLECTED BESSEL	765m	5.68GW

FIGURE 3

TOTAL RADIATED POWER = 6.822 GW
TOTAL POWER FROM RECTENNA = 5.032 GW

STEP	ELEMENTS/ SUBARRAY	POWER DENSITY kw/m²
1	36	22.14
2	30	18.45
3	24	14.76
4	20	12.30
5	16	9.84
6	12	7.38
7	9	5.54
8	8	4.92
9	6	3.69
10	4	2.46

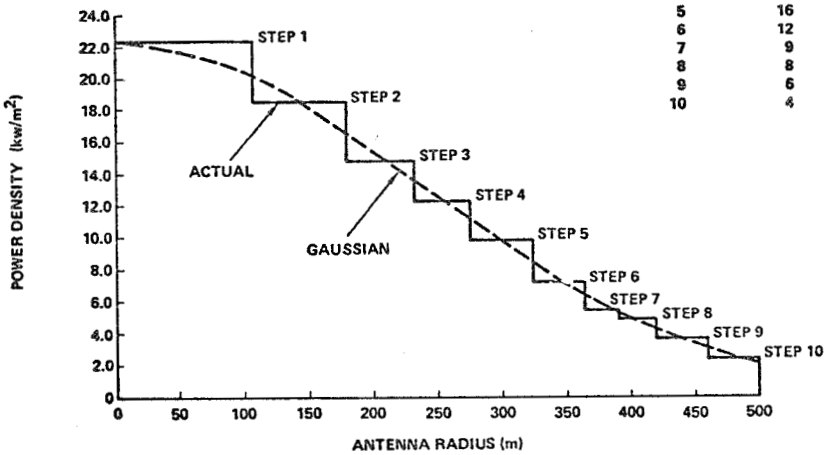

FIGURE 4

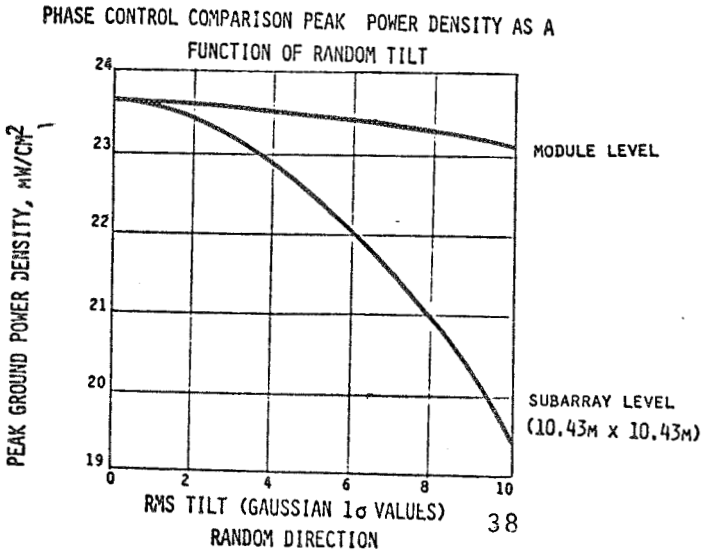

PHASE CONTROL LEVEL COMPUTER SIMULATION

FIGURE 5

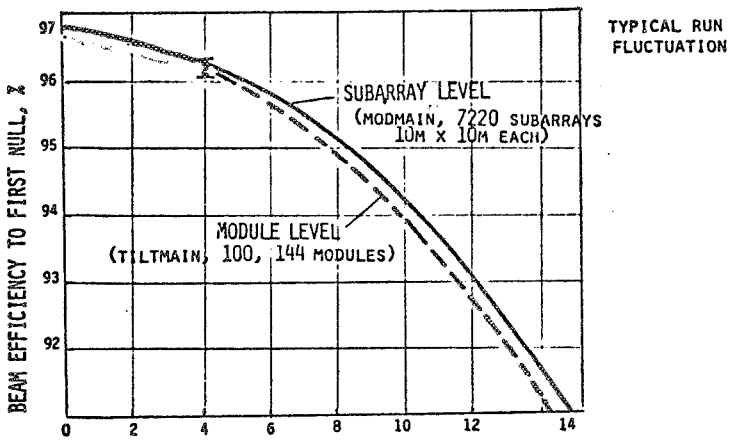

FIGURE 6

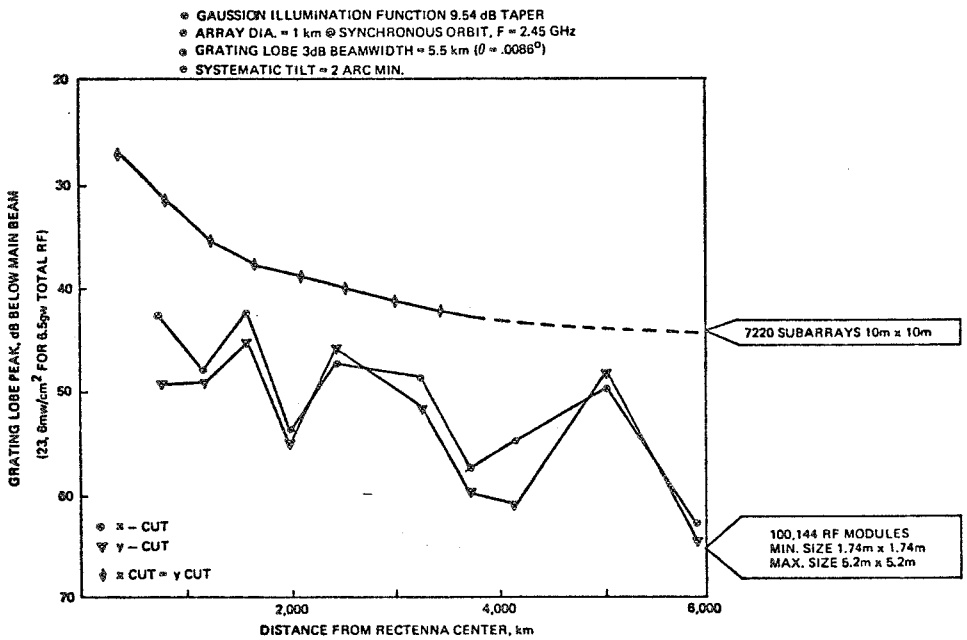

Large Phased Array Simulation of Grating Lobes: Effect of Subarray Size

FIGURE 7

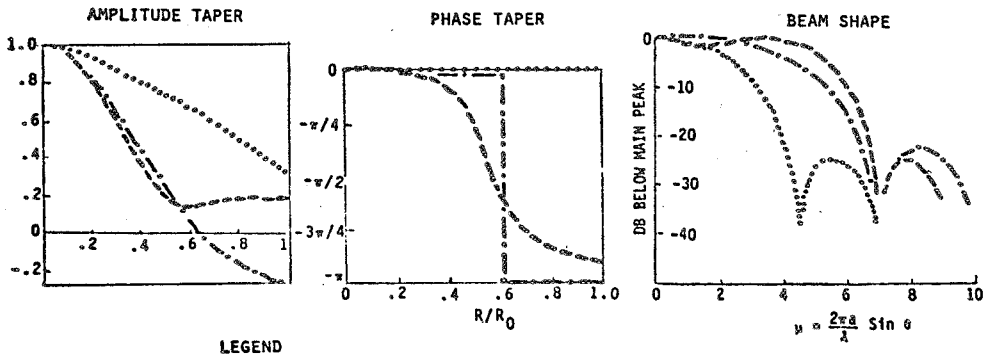

SPS Shaped Beam Synthesis

FIGURE 8

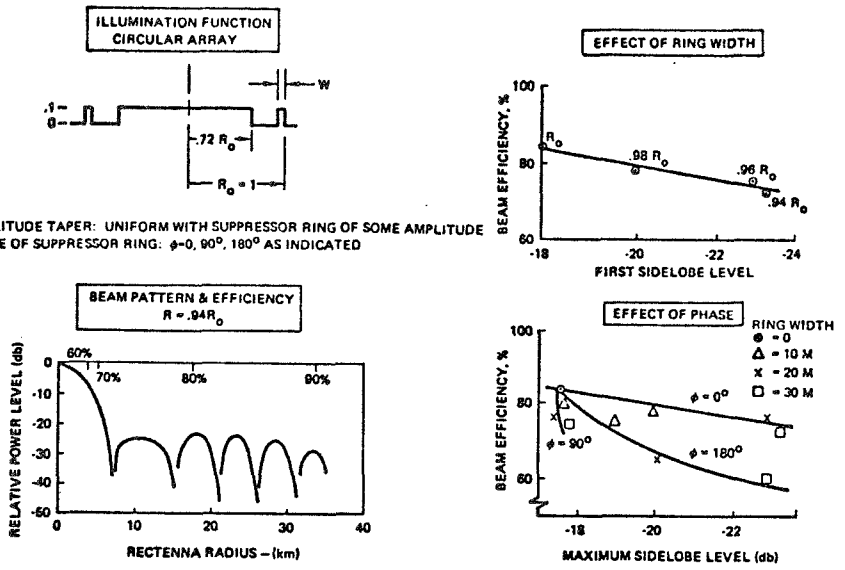

- AMPLITUDE TAPER: UNIFORM WITH SUPPRESSOR RING OF SOME AMPLITUDE
- PHASE OF SUPPRESSOR RING: ϕ=0, 90°, 180° AS INDICATED

DUAL RING

SPACETENNA ILLUMINATION FUNCTION

FIGURE 9

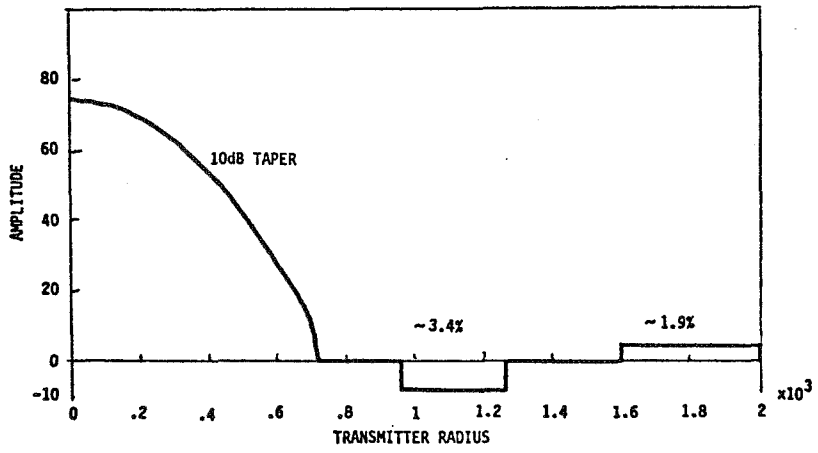

DUAL RING

FAR-FIELD PATTERN

FIGURE 10

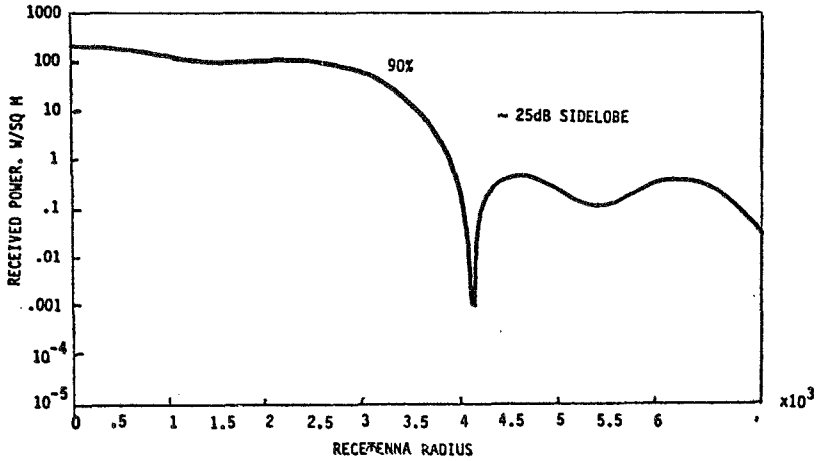

SPS Shaped Beam Synthesis

AMPLITUDE TAPER – UNIFORM
PHASE TAPER – QUADRATIC $\phi = \phi_{MAX}(R/R_O)^2$
SPACE ANTENNA 1 KM DIA., 2.45 GHz 22kw/m^2 5GW

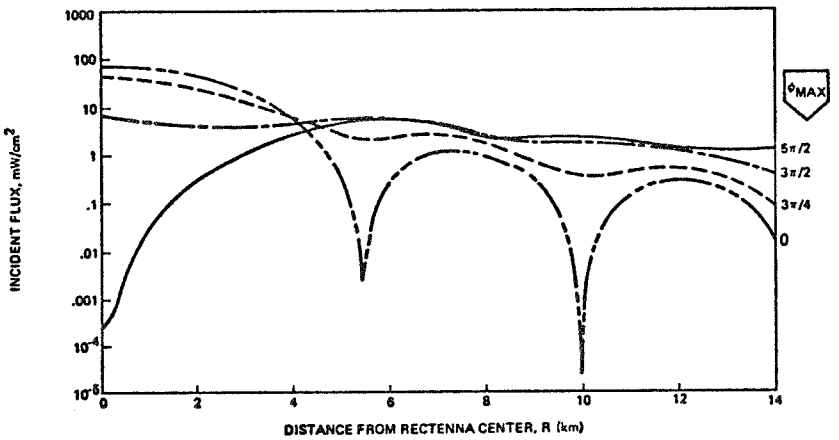

FIGURE 11

SPS Shaped Beam Synthesis

- AMPLITUDE TAPER: UNIFORM
- PHASE TAPER: QUADRATIC, $\phi = \phi_{MAX}(R/R_O)^2$
- SPACE ANTENNA 1 KM DIA., 2.45 GHz

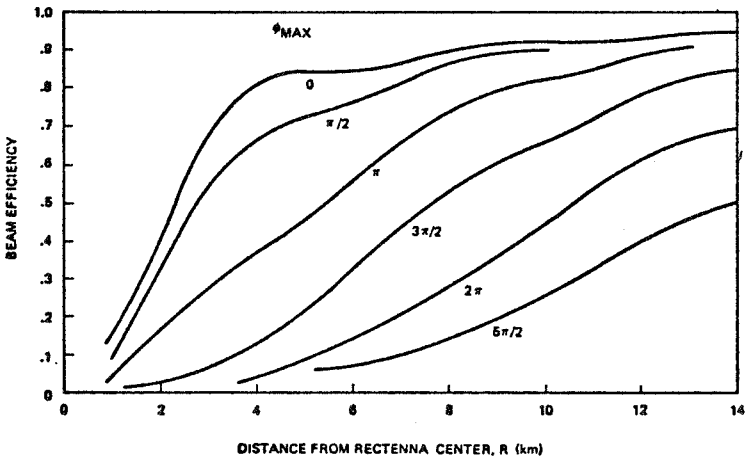

FIGURE 12

SPS Shaped Beam Synthesis

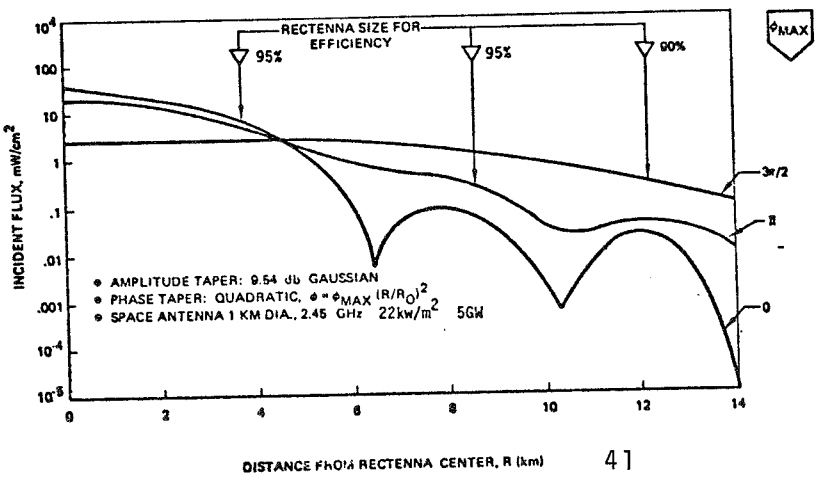

FIGURE 13

FIGURE 14

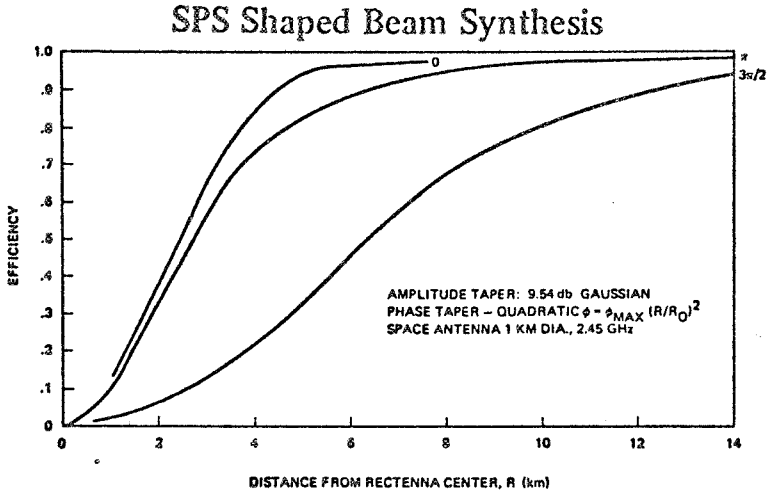

FIGURE 15

ALTERNATE SPS DESIGNS USING BEAM DEFOCUSING
QUADRATIC PHASE TAPER $\phi = \phi\ MAX(R/R_0)^2$

ϕ MAX	PEAK ON AXIS POWER mW/cm^2	RECTENNA DIAM. KM	POWER FLUCTUATION CR. TO EDGE	EFFICIENCY %	
		5GW 1KM 22KW/M^2			
0	23	10KM	23:1	97	← KLYSTRON BASELINE 5GW
1.2π	5.8	22	35:1	95	
3π/2	2.1	28	48:1	92	
		10GW 1.4KM 22KW/M^2			
1.2π	23	15.7KM	35:1	95	← POTENTIAL 10GW KLYSTRON DESIGN
		2GW 1.5KM 5KW/M^2			
1.2π	20	6.7	23:1	97	← SOLID STATE SPS (BOEING)-2GW
	5.8	14.7	35:1	95	
		4GW 2.1KM 5KW/M^2			
1.2π	20	10.5	35:1	95	← POTENTIAL SPS 4GW DESIGN

FIGURE 16